MIPAS database: Validation of HNO3 line parameters using MIPAS satellite measurements

J.-M. Flaud, G. Brizzi, M. Carlotti, A. Perrin, M. Ridolfi

Atmos. Chem. Phys., 6, 5037–5048, 2006
www.atmos-chem-phys.net/6/5037/2006/

Atmospheric Chemistry and Physics

MIPAS database: Validation of HNO_3 line parameters using MIPAS satellite measurements

J.-M. Flaud[1], G. Brizzi[2], M. Carlotti[2], A. Perrin[1], and M. Ridolfi[2]

[1]Laboratoire Interuniversitaire des Systèmes Atmosphériques (LISA), CNRS, Universités Paris 12&7, 61 avenue du Général de Gaulle, 94010 Créteil Cedex, France
[2]Dipartimento di Chimica Fisica e Inorganica, Università di Bologna, Viale del Risorgimento, 4, 40136 Bologna, Italia

Received: 16 January 2006 – Published in Atmos. Chem. Phys. Discuss.: 29 May 2006
Revised: 21 September 2006 – Accepted: 30 October 2006 – Published: 3 November 2006

Abstract. Using new and accurate experimental results concerning the spectroscopic properties of the HNO_3 molecule as well as improved theoretical methods it has been possible to generate an improved set of line parameters for this molecule in the spectral range covered by the MIPAS (Michelson Interferometer for Passive Atmospheric Sounding) experiment. These line parameters, which have been validated using broadband atmospheric spectra recorded by MIPAS, have been included in the last version of the MIPAS spectroscopic database to be used for future processing of the MIPAS spectra.

1 Introduction

The goal of this study, which concerns the line positions, the line intensities and the broadening coefficients of the HNO_3 molecule, is to provide the best and the most consistent possible set of line parameters for the nitric acid molecule in the spectral range covered by the Michelson Interferometer for Passive Atmospheric Sounding (MIPAS) (Endemann, 1999). In a previous effort which has led to the MIPAS_PF3.1 version of the database (Flaud et al., 2003a) the spectral parameters of the hot band $\nu_5+\nu_9-\nu_9$ were improved using both laboratory spectra and atmospheric spectra recorded by the Atmospheric Trace MOlecule Spectroscopy (ATMOS) experiment (Flaud et al., 2003b). Also to account for new results concerning the intensities in the 11.2 μm region (Toth et al., 2003) the line intensities of the ν_5, $2\nu_9$, ν_3 and ν_4 bands were multiplied by the factor 0.879 (Flaud et al., 2003a). Since that time new results (Chackerian et al., 2003) have been obtained and a careful survey of the literature together with new calculations have shown that new improvements can be made concerning the nitric acid line parameters. Also using broadband emission spectra of the atmosphere recorded by MIPAS it has been possible to validate the consistency of the HNO_3 line parameters in the various spectral ranges covered by the MIPAS experiment. In order to facilitate reading the manuscript we give in Table 1 the usual spectroscopic notation together with the notation used in the MIPAS database as well as in the HITRAN database, up to the 2000 release (Rothman et al., 2003), and the band centers of the cold bands and of some hot bands or combination bands which will be included in the new version PF3.2 of the MIPAS database.

Correspondence to: M. Ridolfi
(marco.ridolfi@unibo.it)

2 Line positions

The line positions have been improved in two spectral regions:

- around 11.2 μm for the ν_5 and the $2\nu_9$ cold bands for which a new extended study has been performed allowing to improve noticeably the P- and R-branch modeling for the high values of the rotational quantum numbers (Perrin et al., 2004);
- around 8.3 μm for the $\nu_8+\nu_9$ and $\nu_6+\nu_7$ bands for which it appears that the HITRAN database is not using the best Hamiltonian constants and energy levels available in the literature (Perrin et al., 1999).

In the 11.2 μm region a new analysis was performed by mixing the existing microwave data and a re-analysis of a series of infrared spectra recorded with different HNO_3 amounts and at various temperatures. Then, using an Hamiltonian model and an intensity model taking fully into account the various vibro-rotational resonances as well as the torsional effects and the axis switching effect, a new line list of positions and intensities (as far as the absolute intensities are concerned see next section) has been generated allowing one to better model the HNO_3 spectrum (Perrin et al., 2004).

Published by Copernicus GmbH on behalf of the European Geosciences Union.

Table 1. Notations and band centers.

Spectroscopic notation	MIPAS_PF3/HITRAN2K notation	Band center (cm^{-1})
Pure rotation	14–14	0.0
ν_9	19–14	458.229
ν_7	31–14	580.304
ν_6	26–14	646.826
ν_8	32–14	763.154
$3\nu_9-\nu_9$	23–19[a]	830.675
$\nu_5+\nu_9-\nu_9$	24–19	885.425
ν_5	18–14	879.108
$2\nu_9$	21–14	896.447
$\nu_8+\nu_9$	33–14	1205.707
$\nu_6+\nu_7$	25–14[b]	1222.679
ν_4	17–14	1303.518
ν_3	27–14	1325.735
ν_2	16–14	1709.568
ν_1	15–14	3550.0

[a] Not included in HITRAN2K
[b] Not included in HITRAN2K and MIPAS_PF3.1 but included in MIPAS_PF3.2

In particular, as it can be seen in Figs. 1 and 2 of Perrin et al. (2004), the new line parameters lead to a significant improvement in the wings of the 11 μm window from which one should now be able to retrieve more accurately the CFC-11 (CCl_3F) and CFC-12 (CCl_2F_2) atmospheric species at $\sim$850 and $\sim$920 cm^{-1}, respectively.

In the 8.3 μm spectral region the line positions and the line intensities included in HITRAN come from a private communication (A. Goldman: $\nu_8+\nu_9$ band, 1990; originally generated by A. G. Maki, based on Maki, 1989) and only the strongest band absorbing in this region, the $\nu_8+\nu_9$, was accounted for, whereas this band is in interaction with another combination band $\nu_6+\nu_7$. This interaction was treated properly by Perrin et al. (1999) who has provided more precise and meaningful Hamiltonian constants. Using these constants allows one to generate a better set of energy levels and hence of line positions.

3 Line intensities

The determination of accurate line intensities for nitric acid is an overarching problem and is still controversial since several previous and ongoing efforts in various laboratories give results which do not agree. The first studies concerned measurements of the integrated band intensities (see Appendix A for the relationship between the integrated band intensity and the cold band intensity) at 11 μm using low resolution spectra (Goldman et al., 1971; Giver et al., 1984; Massie et al., 1985; Hjorth et al., 1987). They led to integrated strengths at 296 K varying from 490 to 638 cm^{-2} atm^{-1} (see Table 2). The situation was not better for individual line intensity measurements since the results obtained using a diode laser technique (Brockman et al., 1978) are on the average 20% lower than those using Fourier transform spectra (Perrin et al., 1993). Also there exists a discrepancy between the low and high resolution measurements. For example the band strength derived at 11 μm from Perrin et al. (1993) is about 30% weaker than the value measured by Giver et al. (1984). All these discrepancies show the difficulty of the problem. Finally it is worth stressing that the recommendation adopted for the preparation of the HITRAN2K database (Rothman et al., 2003) was to normalize the ν_5 and $2\nu_9$ linelist generated in Perrin et al. (1993) to the Giver 11 μm band intensity after a proper hot band correction[1].

Table 2. Comparison of measured HNO_3 integrated band intensities in the 11.2 μm spectral region at 296 K.

References	Integrated band intensity	
	cm^{-2} atm^{-1}	cm^{-1}/(molecule cm^{-2})
Goldman et al. (1971)	592	$2.39(37)\times10^{-17}$ [a]
Giver et al. (1984)	638	$2.57(13)\times10^{-17}$
Massie et al. (1985)	490	$1.98(30)\times10^{-17}$
Hjorth et al. (1987)	548	$2.21(33)\times10^{-17}$

The band intensities are given in the two most commonly used units.
[a] Numbers in brackets are RMS errors.

Very recently two new studies were devoted to the measurement of HNO_3 line intensities at 11 μm:

– an extensive set of HNO_3 individual line intensities (733 and 402 for the ν_5 and $2\nu_9$ bands, respectively) were measured using Fourier transform spectra (Toth et al., 2003). The goal was once again to measure accurate absolute line intensities in the 11 μm region while adopting special experimental precautions to minimize and/or estimate correctly the HNO_3 decomposition. This new list of line intensities is rather complete providing one with a much more extended set of measured intensities and a larger range of rotational quantum numbers than previously (Perrin et al., 1993). On the average these new line intensities are weaker than those in the HITRAN2K linelist: $INT_{HIT2K}/INT_{NEW}\sim1.136\pm0.060$. We used this set of data to normalize the HNO_3 intensities at 11 μm for MIPAS_PF3.1. However it should be noted that the HNO_3 linelist used for MIPAS_PF3.1 was the linelist generated by Perrin et al. (1993) whereas in MIPAS_PF3.2 we used the improved linelist generated by Perrin et al. (2004).

[1] As explained in Appendix A, the integrated band intensity S_{tot} can be related to the intensity of the cold band through the "approximate" relationship: $S_{tot}(T)=S_{cold\,band}(T)*Z_{vib}(T)$. For HNO_3 we use $Z_{vib}(296)=1.29952$.

– Fourier transform absorbances were measured at Pacific Northwest National Laboratory (Chackerian et al., 2003) for different samples of nitrogen-nitric acid mixtures at a spectral resolution of 0.112 cm^{-1} and used to determine integrated cross sections in various spectral domains. For the 11 μm region, the integrated intensity is about 6% lower than the value reported by Giver et al. (1984) and about 7% higher than the intensities derived from the measurements of Toth et al. (2003).

Now, given all these various results one has to decide which sets of experimental intensity data should be used in the MIPAS database. If one performs the arithmetic mean of the experimental results quoted in Table 2 one gets for the integrated total band intensity at 11.2 μm (these experimental results are the more numerous) the following value: $2.29(25)\times10^{-17}$ cm^{-1}/(molecule cm^{-2}). This value, if it has a significant physical meaning, corresponds to the value measured by Toth et al. (2003). Also it is worth stressing that in the validation of the MIPAS nitric acid measurements using far infrared data from the IBEX (Infrared Balloon EXperiment) experiment it is shown that this value gives the best agreement between the two sets of atmospheric measurements (Mencaraglia et al., 2006). As a consequence we retained the Toth et al.'s individual line intensities at 11.2 μm which were fitted (Perrin et al., 2004). Then the corresponding transition moment constants were used to generate the line intensities included in MIPAS_PF3.2.

For the other spectral domains, except the domain 1160–1240 cm^{-1}, there is a reasonable agreement between the Chackerian data and the Giver data; we then scaled the Chackerian et al. (2003) data using the band intensity at 11.2 μm derived from the fit of the Toth et al.'s (2003) data and used the line parameters derived in this way to start the validation process using the MIPAS spectra. The band intensity values quoted in Table 3 for MIPAS_PF3.2 are the values finally retained.

We do not understand the origin of the rather strong discrepancy in the 1160–1240 cm^{-1} spectral domain. One argument could be that some impurity (such as N_2O_5) was existing in the Giver's sample leading to a measured integrated band intensity larger than it would be for a pure nitric acid sample. For this reason we suggest to use in this spectral domain the integrated band intensity value of Chackerian et al. (2003) corrected as explained above. Table 3 gives the band intensities derived from the line parameters included in MIPAS_PF3.1 (Flaud et al., 2003a) and MIPAS_PF3.2. Also it is worth noticing that the HNO_3 line intensities included in the last issue of HITRAN have also been modified. We give then the band intensities of HITRAN2K (Rothman et al., 1998, 2003) as well of HITRAN04 (Rothman et al., 2005).

4 Broadening coefficients

4.1 Self-broadening coefficients

Although the HNO_3 self-broadening coefficients are rather large, their precise knowledge is not really important given the nitric acid atmospheric concentrations. It is suggested to use an average value of 0.807(70) cm^{-1}/atm at 296 K based on the 4 microwave measurements of Zu et al. (2002).

4.2 Air-broadening coefficients

The only existing line broadening calculation was performed some years ago (Tejwani and Yeung, 1978). Since this historical work, which was performed using the Anderson-Tsao-Curnutte theory, to our knowledge no other line broadening calculation has been performed. It is however interesting to notice that, even if the calculations cannot be considered as being accurate, they show a strong dependence of the broadening parameters with respect to the rotational quantum numbers.

As far as experiments are concerned there exist rather few broadening measurements for HNO_3 in the literature. The most accurate were performed in the microwave or submillimeter spectral regions since it is then possible to observe well isolated lines (Goyette et al., 1988, 1991, 1998; Zu et al., 2002; Perrin et al., 2005). Table 7 of Perrin et al. (2005) gives a list of air-broadening coefficients (these coefficients were either measured directly or derived from the N_2- and O_2-broadening coefficients through the classical relationship: γ_{air}(T)=0.79 γ_{N_2}(T)+0.21 γ_{O_2}(T)) for various pure rotational transitions in the microwave or millimeter region.

From Table 7 of Perrin et al. (2005), it is evident that there exists a rather clear rotational dependence of the broadening coefficients which need to be modeled. In the absence of accurate theoretical calculations it was decided (Perrin et al., 2005) to rely on an empirical model which reproduces as well as possible the observed line broadening parameters. It was then proposed to model the rotational dependence of γ_{air} as follows (see Perrin et al., 2005, for more details):

– For $J = (J' + J'')/2$ values $< J^{Max} = 34.5$

$$\gamma_{air}(J) = a_{air} + b_{air} \cdot J$$

with a_{air}=0.1280 cm^{-1} atm^{-1} and b_{air}=−0.0008635 cm^{-1} atm^{-1}.

– For J values $> J^{Max}$

$$\gamma_{air}(J) = \gamma_{air}(J^{Max}) = 0.982\ cm^{-1}/atm \text{ (constant value)}$$

Figure 1 of Perrin et al. (2005) shows that the observed air-broadening coefficients are rather well modeled with the empirical formulae given above. Consequently the air-broadening parameters included in MIPAS_PF3.2 were generated using the above formulae.

Table 3. HNO_3 integrated band intensities.

Range (cm^{-1})	Assignment[a]	Integrated band intensity (cm^{-1}/(molecule cm^{-2}))					
		Chackerian et al. (2003)	Giver et al. (1984)	HITRAN 2K	MIPAS PF3.1	HITRAN 04	MIPAS PF3.2
820–950	18–14, 21–14, 23–19, 24–19	$2.424(65)\times10^{-17}$ [b]	$2.54(13)\times10^{-17}$	2.564×10^{-17}	2.266×10^{-17}	2.267×10^{-17}	2.308×10^{-17}
1160–1240	33–14, 25–14	$1.263(81)\times10^{-18}$	$1.64(15)\times10^{-18}$	1.592×10^{-18}	1.587×10^{-18}	1.589×10^{-18}	1.235×10^{-18}
1240–1400	17–14, 27–14	$5.09(18)\times10^{-17}$	$5.15(26)\times10^{-17}$	4.780×10^{-17}	4.201×10^{-17}	5.095×10^{-17}	4.960×10^{-17}
1480–1570	$\nu_5+\nu_6$, $2\nu_8$	$9.01(81)\times10^{-19}$			0.	0.	0.
1640–1770	16–14	$5.71(19)\times10^{-17}$	$5.70(37)\times10^{-17}$	5.693×10^{-17}	5.693×10^{-17}	5.693×10^{-17}	5.693×10^{-17}
2460–2710	$\nu_2+\nu_5$, $2\nu_3$, $2\nu_4$	$1.42(20)\times10^{-18}$		0.	0.	0.	0.

[a] The assignments are given in HITRAN2K notation when the bands are included in the existing databases, in spectroscopic notation otherwise.
[b] Numbers in brackets are RMS errors.

4.3 Temperature dependence of the line widths

There exist even rather few measurements concerning the temperature dependence of the broadening coefficients (the only n-temperature dependence obtained is n_{N_2}=0.64 to 0.74 and n_{O_2}=0.67 to 0.84 for N_2 and O_2, respectively; Goyette et al., 1991, 1998). From these measurements no clear dependence with respect to the rotational quantum numbers could be derived for the n_{air} coefficient (Perrin et al., 2005). An average value of 0.725(90) can be derived not far from the theoretical value of 0.75. For this reason we suggest to use this last value for the MIPAS_PF3.2 database.

5 Validation of the new database

The new HNO_3 line parameters were validated by comparing MIPAS observed limb-emission radiances with radiances simulated using alternatively the new (PF3.2) and the old (PF3.1) line parameters. The MIPAS observed radiances considered in this validation work (ESA reprocessed data version 4.62) were selected among the observations acquired during the "well-characterized" ENVISAT orbits 2081 and 2082 (from 24 July 2002), with nominal tangent altitudes of 12 and 24 km.

Since our forward model is not able to simulate the effect produced by clouds located within the instrument field-of-view, the observed spectra were preliminarily filtered to exclude the measurements affected by clouds (Remedios et al., 2003). In order to avoid disturbances due to upward error propagation that may take place when retrieving HNO_3 Volume Mixing Ratio (VMR) profiles from limb-scans affected by clouds at low altitudes, whenever a spectrum with tangent altitude equal to or lower than 12 km was detected, the full limb-scan was excluded from our analysis. This filtering process led to the selection of 55 spectra with nominal tangent altitude of 12 km and 55 spectra with nominal tangent altitude of 24 km.

For each of the selected measurements, the corresponding simulation was calculated in the following three spectral intervals affected by the new spectroscopic HNO_3 line data:

a) 840–930 cm^{-1} (sub-interval of MIPAS band A)

b) 1270–1360 cm^{-1} (sub-interval of MIPAS band B)

c) 1670–1740 cm^{-1} (sub-interval of MIPAS band C)

The synthetic spectra were simulated using a modified version of the 2-D forward model implemented in the Geofit code (Carlotti et al., 2001). Beyond the capabilities of the Geofit forward model, the used model includes some additional functionalities, namely:

– modeling of heavy species with tabulated cross-sections,

– modeling of line-mixing, pressure-shift and self-broadening,

– modeling of atmospheric continua due to H_2O, O_2 and N_2,

– capability to simulate spectral intervals as broad as the MIPAS bands.

In all the forward model calculations presented in this paper, the atmospheric composition and the observation geometry were assumed as follows:

– line-of-sight pointing angles, pressure, temperature, and VMR of H_2O, O_3, CH_4, N_2O and NO_2 had the values retrieved by the MIPAS off-line processor (Ridolfi et al., 2000), operated with the MIPAS_PF3.1 spectroscopic database.

– The VMRs of all the other chemical species, but HNO_3, were set equal to their climatological value specific for the month of July and the latitude band to which the observations refer.

Three sets of simulations were calculated, differing for the used HNO_3 spectroscopic database and the HNO_3 VMR profile distributions. Namely, the simulated sets (Sx) of spectra are characterized as follows:

S1: spectroscopic database version PF3.1, HNO_3 VMR profiles retrieved by the MIPAS off-line processor operated with the PF3.1 spectroscopic database;

S2: spectroscopic database version PF3.2, HNO_3 VMR profiles retrieved by the MIPAS off-line processor operated with the PF3.1 spectroscopic database;

S3: spectroscopic database version PF3.2, HNO_3 VMR profiles retrieved by the MIPAS off-line processor operated with the PF3.2 spectroscopic database.

In all cases, the off-line processor used the spectral intervals: 876.375–879.375 cm^{-1} and 885.100–888.100 cm^{-1}. Finally, in order to damp the sidelobes of the instrument response function, both observed and simulated spectra were apodized using the Norton-Beer strong apodization function (Norton and Beer, 1976).

For each of the three simulated sets of spectra, the differences between observations and the corresponding simulations (residuals) were averaged in order to reduce the impact of the measurement noise. Nevertheless, the average residuals widely exceed the noise error expected for the average, especially in MIPAS band A. As we will show in Sect. 5.2, this inconsistency has several causes, among them the erroneous assumption in our simulations of the VMR of some CFCs and the use of an approximate instrument model. All these effects produce an error in the simulated limb-radiances of the same order of magnitude of the measurement noise (about 50 $nW/(cm^{-1}\,sr\,cm^2)$). This error can be hardly appreciated when individual measurements are compared with the related simulations, however the error becomes evident when the noise is reduced by the averaging process. The macroscopic shape of the average residual interferes with the assessment of spectroscopic data, therefore it is desirable to remove from these residuals at least the components that can be attributed to known causes. For this reason, the average residuals were corrected using the Residual and Error Correlation analysis technique summarized hereafter.

5.1 The residual and error correlation analysis

The Residual and Error Correlation (REC) analysis used in this study (A. Dudhia, private communication, 2002) is a technique that permits to characterize objectively a residual spectrum in terms of its consistency with the known error sources that may affect either the observed or the simulated spectra.

In case of perfect agreement between observations and simulations, the residual spectrum consists of only measurement noise. In practical cases however, the inaccuracies of both the atmospheric and the instrument models contribute to build-up a shaped residual spectrum. The features of the residual spectrum depend on the actual errors affecting the measured spectrum (as e.g. the intensity- or frequency-calibration errors) and the simulated spectrum (as e.g. the errors due to model parameter errors). The spectral signatures due to a given error source can be characterized with the so called error-spectrum. The error-spectrum of a particular model- or instrument-parameter is defined as the difference between the synthetic spectrum calculated applying a $1\,\sigma$ perturbation to the considered parameter, and the corresponding spectrum calculated in unperturbed conditions. The observed residual spectrum, represented here by the n-dimensional vector $\mathbf{r}_0$, is the result of independent contributions from the various error sources. Assuming that the effects of the various error components combine linearly, the residual spectrum can be simulated by a linear combination of error spectra. If we arrange the m error spectra of the known error sources as columns of a $(n \times m)$ matrix $\mathbf{E}$, the simulated residual spectrum $\mathbf{r}$ can be calculated as:

$$\mathbf{r} = \mathbf{E}\mathbf{c}\,, \tag{1}$$

where $\mathbf{c}$ is the m-dimensional vector of the coefficients of the linear combination. The coefficients $\mathbf{c}$ generating the simulated residual spectrum that best fits (in the least squares sense) the observed one are obtained as:

$$\mathbf{c} = \left(\mathbf{E}^T\mathbf{S}^{-1}\mathbf{E}\right)^{-1}\mathbf{E}^T\mathbf{S}^{-1}\mathbf{r}_0 \tag{2}$$

where $\mathbf{S}$ is the covariance matrix characterizing the measurement noise of the observed spectrum.

5.2 Correction of the residuals with the REC-analysis

In Fig. 1 we report an example of the average residuals obtained in the selected spectral sub-interval of MIPAS band A, for nominal tangent height of 12 km. In particular, panel (a) of this figure shows the average measured spectrum, panel (b) shows the residual obtained with the average simulation of

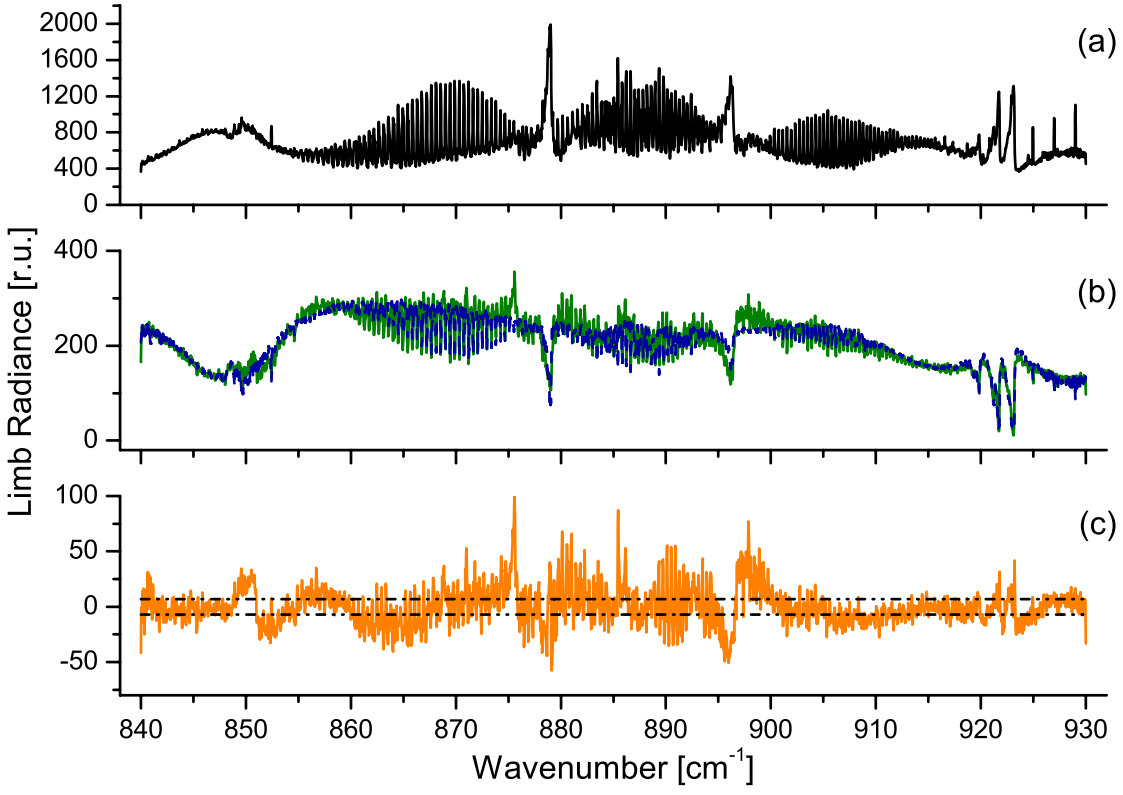

Fig. 1. Example of average residual for a sub-interval of MIPAS band A, at nominal tangent height of 12 km. Panel **(a)** shows the average measured spectrum, panel **(b)** shows the residual obtained with the average simulation of type S2 (green line) and the residual spectrum simulated by the REC-analysis (blue line). Panel **(c)** shows the difference between the two residuals reported in panel (b) (green minus blue). The dashed lines indicate MIPAS measurement noise level for the average: 7 nW/(cm^2 sr cm^{-1}) in this spectral interval.

type S2 (green line) and the residual spectrum simulated by the REC-analysis (blue line). Panel (c) of Fig. 1 shows the difference between the two residuals reported in panel (b) (green minus blue). In Fig. 1 we can see that the REC-analysis is able to capture most of the broadband- as well as some fine-structures of the residuals observed with the S2 simulations. In particular we find that, in this spectral region the residual simulated by the REC-analysis is the linear combination of error spectra relating to:

- VMR of CFC-11, CFC-12 and CFC-22,
- atmospheric continuum model,
- assumed pressure and temperature distributions,
- instrumental offset.

While the linear approximation of the REC-analysis does not permit to estimate accurate corrections for the values of forward- and instrument-model parameters that are responsible for the shaped residual, it is possible to correct the average simulated spectrum by adding to it the REC-analysis simulated residual, hence obtaining a less shaped residual as the one shown in panel (c) of Fig. 1. The corrected residuals permit to highlight with a better contrast their remaining unexplained features.

For the sake of our validation we carried-out the REC-analysis individually, on each of the average residuals obtained from the simulations of type S2, i.e. for each of the three considered spectral intervals and the two tangent heights of 12 and 24 km. The simulated residuals resulting from this REC-analysis were then added to the corresponding average simulated spectra of all types S1, S2 and S3, hence producing corrected residuals. It is worth noting that, since the same correction is applied to all of the three simulation types, possible differences among S1-, S2- and S3-corrected residuals cannot be attributed to the REC-analysis procedure.

Uncorrected average residuals relating to the selected spectral regions in MIPAS bands B and C are much less distorted than the residuals in band A (Fig. 1), therefore we are not showing plots for these spectral intervals. It is worth to mention that the REC-analysis in bands B and C highlighted that:

- in the spectral interval 1270–1360 cm^{-1} only the instrumental offset is relevant;

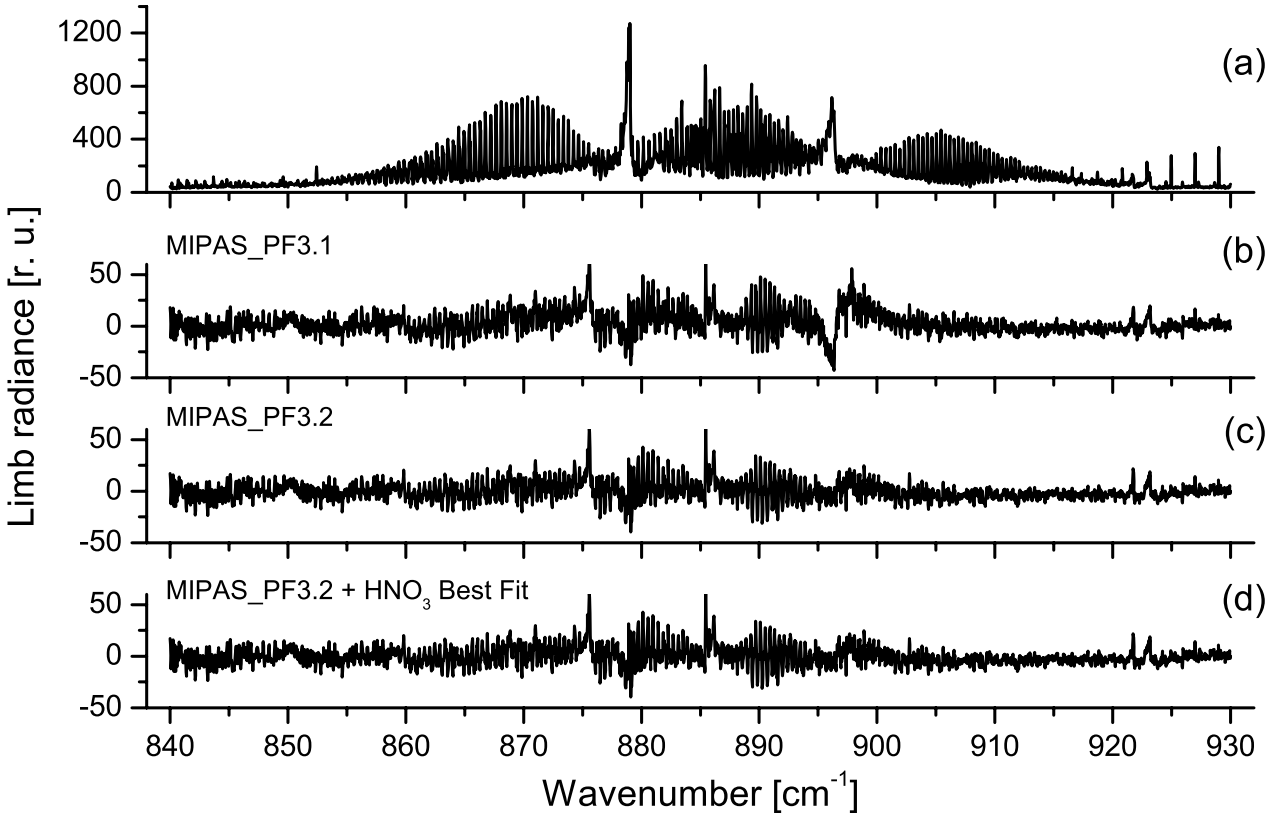

Fig. 2. Panel **(a)**: average of 55 MIPAS spectra acquired during orbits 2081 and 2082 for a sub-interval of band A, at tangent altitude of 24 km. Panels **(b)**, **(c)** and **(d)** show the residuals relating to the REC-corrected average residuals from simulations of type S1, S2 and S3, respectively. The noise level for the average in this spectral interval is about 7 nW/(cm^2 sr cm^{-1}).

– in the spectral interval 1670–1740 cm^{-1} the important error sources are: VMR of $ClONO_2$ and instrument model errors such as instrument line-shape distortion, radiometric gain, offset and frequency calibrations.

5.3 Analysis of the corrected residuals

The REC-analysis corrected average residuals were characterized individually, for each considered spectral interval and tangent height, in terms of both their average and root mean square (RMS) deviation.

Table 4 presents the results of this analysis. First, it is easy to recognize (see rows of Table 4 with bold entries) that for the two selected spectral intervals in MIPAS bands A and B, at both tangent heights, the new database provides results better than the old one in terms of both average value and RMS of the residuals. The line database changes, however, have only a marginal impact on the residual in band C. Furthermore, we can also see that, while using for the simulation the new HNO_3 line data, the residual changes only very marginally if we use the HNO_3 VMR distribution retrieved either with the old or the new line data (compare Table 4 rows with label "3.2" and "3.2^c" on the first column). This is due to the fact that in the microwindows used for the retrievals the old and the new HNO_3 line data are not very different.

A "visual" confirmation of these findings can be found in the plots presented in Figs. 2 and 3 referring to the selected spectral intervals in bands A and B respectively, and to the tangent height of 24 km, where the HNO_3 concentration is near its maximum. In these figures panels (a) show the average observed spectrum, while panels (b), (c) and (d) show the average REC-corrected residuals obtained from simulations of types S1, S2 and S3, respectively. Note that, since the achieved improvements are less visible at 12 km (less HNO_3 amount), we are not showing plots of the residuals for this altitude.

The marginal changes of the residual obtained when moving from simulations S2 to simulations S3 hint at the fact that in practice, when moving from the old to the new HNO_3 line data, the retrieved HNO_3 VMR distribution is not changing dramatically. In Fig. 4 we show the average HNO_3 profiles (panel a) retrieved from the MIPAS measurements considered in this work, using the old (solid line) and the new (dashed line) HNO_3 line data. Panel (b) of Fig. 4 shows the percentage differences between these two average profiles: these amount to about 1–1.2 % (i.e. using the old HNO_3

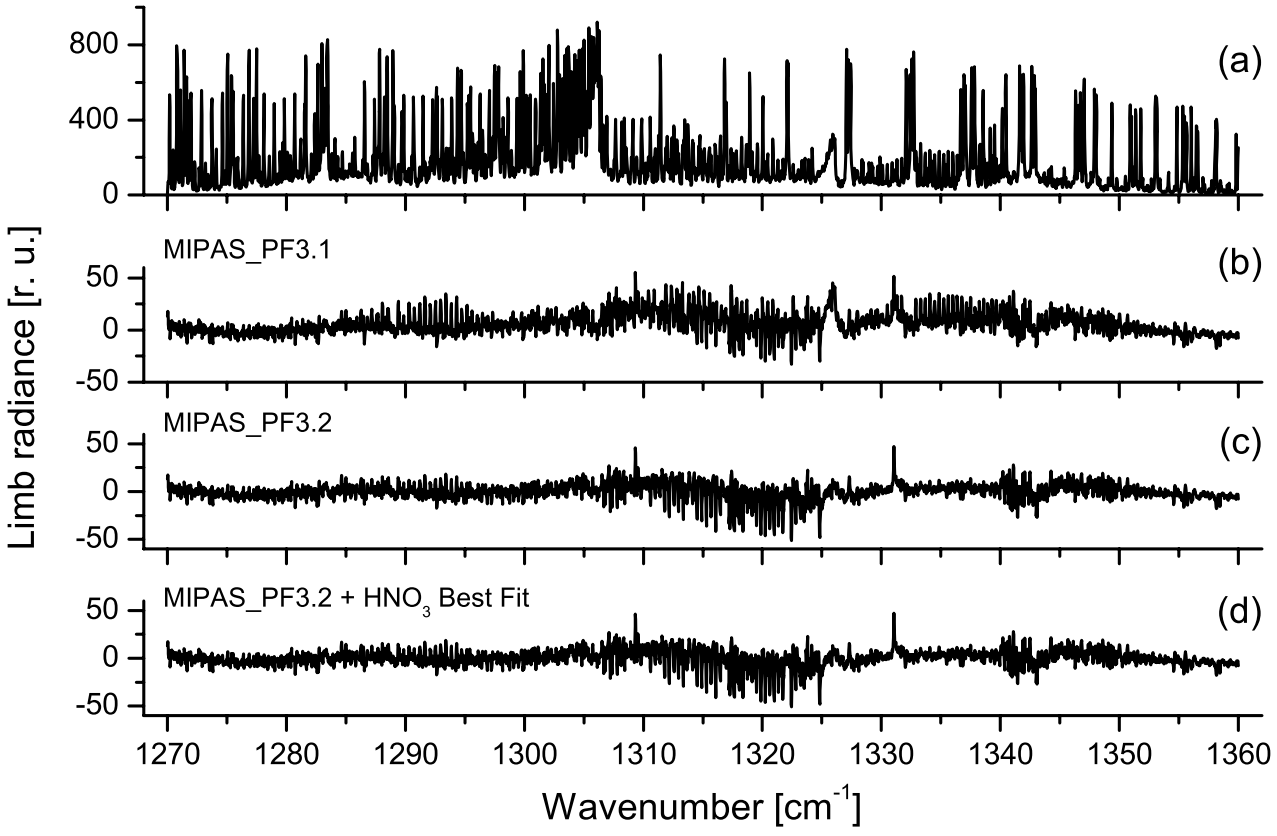

Fig. 3. Panel a): average of 55 MIPAS spectra acquired during orbits 2081 and 2082 for a sub-interval of band B, at tangent altitude of 24 km. The format is the same as in Fig. 2. The NESR of the average in this spectral interval is about 3 nW/(cm^2 sr cm^{-1}).

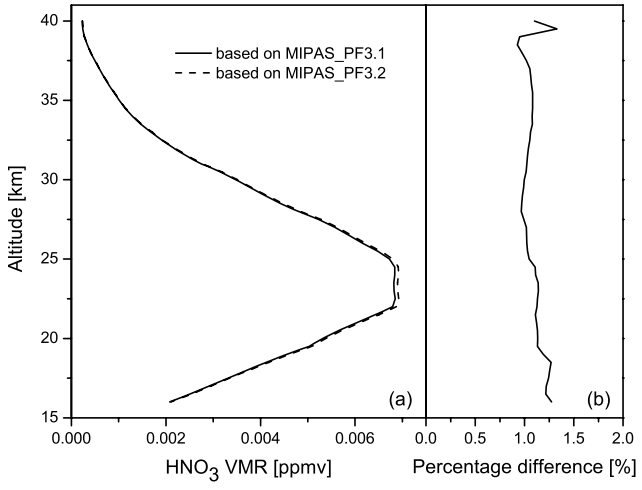

Fig. 4. Average HNO_3 VMR profiles retrieved using MIPAS_PF3.1 and PF3.2 spectroscopic databases (panel **a**) and percentage differences (panel **b**).

database the retrieved VMR profiles turn-out to be systematically underestimated by this amount) and are almost independent from the altitude. As expected from the analysis of the residuals, these differences are small if compared with the random error (≈6%) with which the HNO_3 VMR is usually retrieved from the individual limb-scans of MIPAS. However the obtained differences are purely systematic and therefore become extremely important when large sets (more than about 25) of HNO_3 VMR profiles are averaged.

Beyond the improvements of the residuals achieved with the new line database, some considerations are wise regarding the overall quality of the residuals. In particular we discuss the consistency of the improved residuals with the related Noise Equivalent Spectral Radiance (NESR). As indicated in Table 4, the NESR relating to the average residuals in bands A, B and C is respectively 7, 3 and 0.9 nW/(cm^2 sr cm^{-1}), independent of altitude. Therefore, comparing the RMS of our "best" obtained residuals (from simulations of type S3) with the related NESR it turns-out that:

– Band A: we have to distinguish between the two considered altitudes. At 24 km the RMS of the residual (≈ 9 nW/(cm^2 sr cm^{-1})) is mostly consistent with the related NESR, while at 12 km the RMS of the residual (≈14 nW/(cm^2 sr cm^{-1})) exceeds the related NESR

Table 4. Results of the comparison of MIPAS observed and simulated spectra for tangent heights of 12 and 24 km.

MIPAS database version	Scaling factor	MIPAS band[a]	Spectral interval (cm^{-1})	Tangent Height: 12 km Average difference[b] (r.u.)	RMS (r.u.)	Tangent Height: 24 km Average difference (r.u.)	RMS (r.u.)
3.1	**1.0**	**A**	**840–930**	**5.94**	**17.29**	**2.91**	**11.02**
3.2	**1.0**	**A**	**840–930**	**0.00**	**13.95**	**0.00**	**9.09**
3.2[c]	**1.0**	**A**	**840–930**	**−0.14**	**13.95**	**−0.02**	**9.09**
3.2	0.96	B	1270–1360	1.06	9.85	1.49	9.98
3.2	0.98	B	1270–1360	0.53	9.63	0.74	9.93
3.1	**1.0**	**B**	**1270–1360**	**4.45**	**11.79**	**6.12**	**10.32**
3.2	**1.0**	**B**	**1270–1360**	**0.00**	**9.00**	**0.00**	**8.65**
3.2[c]	**1.0**	**B**	**1270–1360**	**-1.39**	**8.58**	**0.08**	**8.64**
3.2	1.02	B	1270–1360	−0.52	8.85	−0.74	8.70
3.2	1.04	B	1270–1360	−1.04	8.75	−1.47	8.82
3.2	0.96	C	1670–1740	0.24	1.35	0.31	1.27
3.2	0.98	C	1670–1740	0.12	1.30	0.15	1.25
3.1	**1.0**	**C**	**1670–1740**	**0.10**	**1.22**	**0.07**	**1.14**
3.2	**1.0**	**C**	**1670–1740**	**0.00**	**1.21**	**0.00**	**1.15**
3.2[c]	**1.0**	**C**	**1670–1740**	**-0.19**	**1.17**	**0.01**	**1.15**
3.2	1.02	C	1670–1740	−0.12	1.18	−0.15	1.16
3.2	1.04	C	1670–1740	−0.23	1.16	−0.31	1.19

[a] NESR levels of the average MIPAS spectra in bands A, B and C are respectively 7, 3 and 0.9 nW/(cm^2 sr cm^{-1}).
[b] r.u.: Radiance Units, nW/(cm^2 sr cm^{-1}).
[c] Best fit simulation generated with HNO_3 VMR profiles retrieved using MIPAS_PF3.2.

by about a factor of two. We suspect that, despite the use of a cloud detection scheme, at this altitude the effect of unmodeled clouds may still play an important role in building-up large residuals in band A, where the spectrum is the most sensitive to the presence of clouds in the instrument field-of-view. This conclusion is also supported by the recent findings of the MIPAS data products validation activities that presently are still on-going (see individual validation papers in this special issue).

The visual inspection (see Fig. 2 for 24 km altitude) reveals that the large RMS is also due to localized "shaped" residuals. According to the REC-analysis, the uncorrected features in this band can only be attributed to remaining deficiencies in the HNO_3 spectroscopic data. For the peak at 885.4 cm^{-1} we think that the large residual is because no line-mixing effects were introduced in the calculation leading to an approximate modeling of the Q-branch of $\nu_5+\nu_9-\nu_9$ which is extremely narrow. We believe also that the peak at 875 cm^{-1} is due to a missing hot band likely $\nu_5+\nu_6-\nu_6$ or possibly $\nu_5+\nu_7-\nu_7$ (McGraw et al., 1965).

– Band B: in the considered spectral interval the RMS of the residuals ($\approx$ 8.62 nW/(cm^2 sr cm^{-1})) is still greater than the NESR by a factor of about three. Also in this case we attribute the remaining features of the residual to further uncorrected deficiences in the HNO_3 spectroscopic data (see also Fig. 3 for 24 km tangent altitude). This is due to the fact that the spectroscopic modeling of the ν_3 and ν_4 bands is far from perfect due to a lot of resonances to be accounted for (Perrin et al., 1993, and references therein).

– Band C: at both the considered altitudes, 12 and 24 km, the RMS of the residuals ($\approx$1.16 nW/(cm^2 sr cm^{-1})) is mostly consistent with the related NESR. The visual inspection of the residual (not shown here) does not reveal any "localized" problem.

This analysis leads to argue that, while this work implied a significant improvement of the HNO_3 line parameters, the modeling of MIPAS limb-emission spectra would certainly benefit of further spectroscopic line data improvements.

5.4 Inter-band calibration

To go one step further we have tried to see if using the MIPAS spectra it could be possible to improve the consistency of the HNO_3 intensities in the different spectral ranges. For that we have assumed that the line intensities in band A were

Table 5. HNO_3 line parameters in MIPAS_PF3.2.

BAND[a]	XMIN[b]	XMAX[b]	SMIN[c]	SMAX[c]	STOT[d]	NB[e]
31 14	600.0003	613.6181	0.2425D-22	0.1652D-21	0.6853D-19	1200
26 14	615.0260	677.9806	0.2830D-22	0.8540D-21	0.1262D-17	8379
32 14	722.5331	809.9647	0.1211D-22	0.1090D-20	0.1242D-17	7101
23 19	769.6870	884.4384	0.3838D-24	0.6717D-21	0.5290D-18	17720
18 14	806.2073	963.9949	0.9830D-24	0.6600D-20	0.1027D-16	57108
21 14	806.7087	963.4347	0.9830D-24	0.3880D-20	0.7503D-17	55310
24 19	832.1165	942.9013	0.9870D-24	0.7000D-21	0.1067D-17	14521
27 14	1098.3760	1387.8490	0.1037D-22	0.3133D-19	0.2537D-16	21308
3314	1133.5516	1258.8061	0.3706D-24	0.4448D-21	0.9284D-18	40 119
2514	1147.5084	1250.1141	0.3713D-24	0.3535D-22	0.1570D-20	559
1714	1229.8670	1387.5610	0.1037D-22	0.1867D-19	0.1277D-16	19 584
1614	1650.0136	1769.9822	0.2119D-23	0.2119D-19	0.4381D-16	32340

[a] Band notation in the HITRAN2K format (see Table 1)
[b] Lower and higher line position for the band
[c] Lower and higher line intensity for the band
[d] Total band intensity
[e] Number of transitions for the band

correct and we have repeated the simulations of type S2 by multiplying the HNO_3 intensities in bands B and C by factors ranging from 0.96 to 1.04. The resulting average residuals were then corrected with the same REC-simulated residual used in the previous analysis, the average value and the RMS of these residuals are reported in column 2 of Table 4. We find that, when multiplying the HNO_3 intensities by factors of the order 1.02 or 1.04, in both bands the average residuals decrease, corresponding to a general improvement of the residuals because the offset correction provided by the REC-analysis is always greater than +3 nW/(cm^2 sr cm^{-1}). On the other hand, depending on the considered altitude, the corresponding RMS are either decreasing (12 km) or increasing (24 km). In fact we think that, since the residuals include contributions from other atmospheric species which are not perfectly modeled, the decrease of the average differences is due to the increased HNO_3 contributions that compensate some deficiencies in the modeling of the other species. As a consequence it is not possible to improve the consistency of the HNO_3 line parameters in the various MIPAS bands. However one can say that the HNO_3 line intensities are consistent to within 4–5%.

An alternative method that could be used for inter-band calibration would consist in comparing the average HNO_3 VMR profiles retrieved from spectral features in the individual bands. As reported in Fig. 3 of Rothman et al. (2005), this method was successfully applied by Boone and Bernath in 2004 to the occultation measurements of the Atmospheric Chemistry Experiment. In the case of MIPAS, however, the error budget of the HNO_3 VMR (Dudhia, 2005) contains large band-dependent systematic components that would make the ratio between profiles retrieved from the different bands affected by a systematic error greater than the inter-band calibration factor we would like to identify.

Table 5 gives detailed information on the new HNO_3 line parameters included in the last version of the MIPAS database (MIPAS_PF3.2).

6 Conclusion and update of the MIPAS database

Using the most recent and precise experimental results concerning HNO_3 spectroscopic parameters as well as improved theoretical methods it has been possible to generate an improved set of line parameters for this molecule in the spectral range covered by the MIPAS experiment. These line parameters have been validated using broadband atmospheric spectra recorded by MIPAS and have been included in the last version of the MIPAS database MIPAS_PF3.2. The new HNO_3 line data will also be provided to the HITRAN database community.

The analysis of the improved residuals, obtained after the update of the HNO_3 line data, shows that further improvements of the line parameters of this molecule would still be desirable.

Appendix A

The line intensity (in cm^{-1}/(molecule cm^{-2})) for a given vibration-rotation transition is given by the following expression:

$$k = \left(\frac{8\pi^3\nu}{3hc4\pi\varepsilon_0}\right)\exp\left(-\frac{E_L}{kT}\right) \quad \text{(A1)}$$

$$\times[1-\exp(-\frac{hc\nu}{kT})]\frac{1}{Z(T)}|<\Psi''|\mu|\Psi'>|^2$$

where $<\Psi''|\mu|\Psi'>$ is the matrix element of the transition dipole moment operator corresponding to the band, $Z(T)$ is the rotation-vibration partition function calculated at the temperature T. E_U and E_L are the upper and lower energy levels of the transition and ν is the line position.

If the assumption that rotation and vibration can be separated is valid it is possible to sum all the rotational transitions belonging to a single band to get the vibrational band intensity given by:

$$S_{\rm vib}=(\frac{8\pi^3\nu_v}{3hc4\pi\varepsilon_0})\exp(-\frac{E_L^v}{kT})[1-\exp(-\frac{hc\nu_v}{kT})] \quad \text{(A2)}$$
$$\times\frac{1}{Z_{\rm vib}(T)}|<\Psi_v''|\mu|\Psi_v'>|^2$$

where ν_v is the band center, $Z_{\rm vib}(T)$ is the vibrational partition function and $|<\Psi_v''|\mu|\Psi_v'>|^2$ is the vibrational transition moment squared. For a given vibrational mode one has:

$$Z_{\rm vib}(T)=\Pi[1/(1-\exp(-E_v/kT))]$$

In the harmonic approximation $|<\Psi_v''|\mu|\Psi_v'>|^2$ is equal to $(v_i{+}1)\,(\partial\mu/\partial q_i)^2$ where $\partial\mu/\partial q_i$ is the change in dipole moment with respect to the normal coordinate q_i. Also in the harmonic approximation $E^v{=}v_i\omega_i$ and $\nu_v{=}\nu_0$ the band center of the cold band.

Accordingly, the intensity of a given band can be written as:

$$S_{v\leftarrow v+1}=(\frac{8\pi^3\nu_0}{3hc4\pi\varepsilon_0})\exp(-\frac{v\omega}{kT})[1-\exp(-\frac{\omega}{kT})] \quad \text{(A3)}$$
$$\times\frac{(v+1)}{Z_{\rm vib}(T)}(\frac{\partial\mu}{\partial q_i})^2$$

or

$$S_{v\leftarrow v+1}=(\frac{8\pi^3\nu_0}{3hc4\pi\varepsilon_0}) \quad \text{(A4)}$$
$$\times[\exp(-\frac{v\omega}{kT})-\exp(-(\frac{(v+1)\omega}{kT})]\frac{(v+1)}{Z_{\rm vib}(T)}(\frac{\partial\mu}{\partial q_i})^2$$

The integrated band intensity $S_{\rm tot}{=}\sum S_{v\leftarrow v+1}$ is then given by:

$$S_{\rm tot}=(\frac{8\pi^3\nu_0}{3hc4\pi\varepsilon_0})(\frac{\partial\mu}{\partial q_i})^2\frac{1}{Z_{\rm vib}(T)}\sum\exp(-\frac{v\omega}{kT})= \quad \text{(A5)}$$
$$=(\frac{8\pi^3\nu_0}{3hc4\pi\varepsilon_0})(\frac{\partial\mu}{\partial q_i})^2$$

On the other hand the intensity of the cold band $S_{\rm cold\,band}$ is equal to:

$$S_{\rm cold\,band}=(\frac{8\pi^3\nu_v}{3hc4\pi\varepsilon_0})(\frac{\partial\mu}{\partial q_i})^2 \quad \text{(A6)}$$
$$\times[1-\exp(-\frac{\omega}{kT})]\frac{1}{Z_{\rm vib}(T)}$$

Combining Eq. (A5) and Eq. (A6) leads to:

$$S_{\rm tot}=S_{\rm cold\,band}\times \quad \text{(A7)}$$
$$\frac{Z_{\rm vib}(T)}{[1-\exp(-E_U^{v=1}/kT)]}\sim S_{\rm cold\,band}\times Z_{\rm vib}(T)$$

As a consequence it is possible to use Eq. (A7) to link the intensity of the cold band with the integrated band intensity knowing the vibrational partition function (for HNO_3 $Z_{\rm vib}(296)$=1.29952 according to the band centers given in Table 1).

Acknowledgements. The authors are grateful to A. Dudhia from Oxford University for providing the error spectra used in this study.

Edited by: U. Pöschl

References

Brockman, P., Bair, C. H., and Allario, F.: High resolution spectral measurement of the HNO_3 11.3-micron band using tunable diode lasers, Appl. Opt., 17, 91–100, 1978.

Carlotti, M., Dinelli, B. M., Raspollini, P., and Ridolfi, M.: Geofit approach to the analysis of satellite limb-scanning measurements, Appl. Opt., 40, 1872–1875, 2001.

Chackerian, C., Sharpe, S. W., and Blake, T. A.: Anhydrous nitric acid absolute integrated absorption cross sections: 820–5300 cm^{-1}, J. Quant. Spectrosc. Ra., 82, 429–441, 2003.

Dudhia, A.: MIPAS-related section of the web-site of the Oxford University: http://www.atm.ox.ac.uk/group/mipas/err/, 2005.

Endemann, M.: MIPAS instrument concept and performance, Proceedings of the ESAMS'99, ESTEC-ESA, WPP-161, 1, 29–43, ISSN 1022-6656, 1999.

Flaud, J.-M., Piccolo, C., Carli, B., Perrin, A., Coudert, L. H., Teffo, J.-L., and Brown, L. R.: Molecular line parameters for the MIPAS (Michelson Interferometer for Passive Atmospheric Sounding) experiment, Atmos. Oceanic Opt., 16, 172–182, 2003a.

Flaud, J.-M., Perrin, A., Orphal, J., Kou, Q., Flaud, P.-M., Dutkiewicz, Z., and Piccolo, C.: New analysis of the $\nu_5+\nu_9-\nu_9$ hot band of HNO_3, J. Quant. Spectrosc. Ra., 77, 355–364, 2003b.

Giver, L. P., Valero, F. P. J., Goorvitch, D., and Bonomo, F. S.: Nitric-acid band intensities and band-model parameters from 610 to 1760 cm^{-1}, J. Opt. Soc. Am. B, 1, 715–722, 1984.

Goldman, A., Kyle, T. G., and Bonomo, F. S.: Statistical band model parameters and integrated intensities for the 5.9-μ, 7.5-μ, and 11.3-μ bands of HNO_3 vapor, Appl. Opt., 10, 65–73, 1971.

Goyette, T. M., Ebenstein, W. L., De Lucia, F. C., and Helminger, P.: Pressure broadening of the millimeter and submillimeter wave spectra of nitric acid by oxygen and nitrogen, J. Mol. Spectrosc., 128, 108–116, 1988.

Goyette, T. M., Guo, W., De Lucia, F. C., and Helminger, P.: Variable temperature pressure broadening of HNO_3 in the millimeter wave spectral region, J. Quant. Spectrosc. Ra., 46, 293–297, 1991.

Goyette, T. M., Cohen, E. A., and De Lucia, F. C.: Pressure broadening of HNO_3 by N_2 and O_2: an intercomparison in the millimeter wave spectral range, J. Quant. Spectrosc. Ra., 60, 77–84, 1998.

Hjorth, J., Ottobrini, G., Cappellani, F., and Restelli, G.: A Fourier transform infrared study of the rate constant of the homogeneous gas-phase reaction N_2O_5 + H_2O and determination of absolute infrared band intensities of N_2O_5 and HNO_3, J. Phys. Chem., 91, 1565–1568, 1987.

Maki, A.: Infrared Spectrum of the 1205 cm^{-1} band of HNO_3, J. Mol. Spectrosc., 136, 105–108, 1989.

Massie, S. T., Goldman, A., Murcray, D. G., and Gille, J. C.: Approximate absorption cross sections of F12, F11, $C1ONO_2$, N_2O_5, HNO_3, CCl_4, CF_4, F21, F113, F114, and HNO_4, Appl. Opt., 24, 3426–3427, 1985.

McGraw, G. E., Bernitt, D. L., and Hisatsune, I. C.: Vibrational spectra of isotopic nitrics acids, J. Chem. Phys., 42, 237–244, 1965.

Mencaraglia, F., Bianchini, G., Boscaleri, A., Carli, B., Ceccherini, S., Raspollini, P., Perrin, A., and Flaud, J.-M.: Validation of MIPAS satellite measurements of HNO_3 using comparison of rotational and vibrational spectroscopy, J. Geophys. Res., 111, D19305, doi:10.1029/2005JD006099, 2006.

Norton, R. H. and Beer, R.: New apodizing functions for Fourier spectrometry, J. Opt. Soc. Am. 66, 259–264, 1976; errata 67, 419, 1977.

Perrin, A., Flaud, J.-M., Camy-Peyret, C., Jaouen, V., Farrenq, R., Guelachvili, G., Kou, Q., Le-Roy, V., Morillon-Chapey, M., Orphal, J., Badaoui, M., Mandin, J.-Y., and Dana, V.: Line intensities in the 11- and 7.6-μm band of HNO_3, J. Mol. Spectrosc., 160, 524–532, 1993.

Perrin, A., Flaud, J.-M., Keller, F., Goldman, A., Blatherwick, R. D., Murcray, F. J., and Rinsland, C. P.: Analysis of the $\nu_8+\nu_9$ band of HNO_3: line positions and intensities, and resonances involving the v_6=v_7=1 dark state, J. Mol. Spectrosc., 194, 113–123, 1999.

Perrin, A., Orphal, J., Flaud, J.-M., Klee, S., Mellau, G., Mäder, H., Walbrodt, D., and Winnewisser, M.: New analysis of the ν_5 and $2\nu_9$ bands of HNO_3 by infrared and millimeter wave techniques: line positions and intensities, J. Mol. Spectrosc., 228, 375–391, 2004.

Perrin, A., Puzzarini, C., Colmont, J.-M., Verdes, C., Wlodarczak, G., Cazzoli, G., Buehler, S., Flaud, J.-M., and Demaison, J.: Molecular Line Parameters for the "MASTER" (Millimeter Wave Acquisitions for Stratosphere/Troposphere Exchange Research) Database, J. Atmos. Chem., 51, 161–205, 2005.

Remedios, J. J., Spang, R., and Ridolfi, M.: Detection of cloud effects in MIPAS observations and implementation in the operational processor, PO-TN-ULE-GS-0002, technical report of ESA contract 11717/95/NL/CN, 2003.

Ridolfi, M., Carli, B., Carlotti, M., von Clarmann, T., Dinelli, B. M., Dudhia, A., Flaud, J.-M., Hoepfner, M., Morris, P. E., Raspollini, P., Stiller, G., and Wells, R. J.: Optimized forward model and retrieval scheme for MIPAS near-real-time data processing, Appl. Opt., 39, 1323–1340, 2000.

Rothman, L. S., Rinsland, C. P., Goldman, A., Massie, S. T., Edwards, D. P., Flaud, J.-M., Perrin, A., Camy-Peyret, C., Dana, V., Mandin, J.-Y., Schroeder, J., McCann, A., Gamache, R. R., Wattson, R. B., Yoshino, K., Chance, K. V., Jucks, K. W., Brown, L. R., Nemtchinov, V., and Varanasi, P.: The HITRAN Molecular Spectroscopic Database and HAWKS (HITRAN Atmospheric Workstation): 1996 Edition, J. Quant. Spectrosc. Ra., 60, 665–710, 1998.

Rothman, L. S., Barbe, A., Chris Benner, D., Brown, L. R., Camy-Peyret, C., Carleer, M. R., Chance, K., Clerbaux, C., Dana, V., Devc, V. M., Fayt, A., Flaud, J.-M., Gamache, R. R., Goldman, A., Jacquemart, D., Jucks, K. W., Lafferty, W. J., Mandin, J.-Y., Massie, S. T., Nemtchinov, V., Newnham, D. A., Perrin, A., Rinsland, C. P., Schroeder, J., Smith, K. M., Smith, M. A. H., Tang, K., Toth, R. A., Vander Auwera, J., Varanasi, P., and Yoshino, K.: The HITRAN molecular spectroscopic database: edition of 2000 including updates through 2001, J. Quant. Spectrosc. Ra., 82, 5–44, 2003.

Rothman, L. S., Jacquemart, D., Barbe, A., Chris Benner, D., Birk, M., Brown, L. R., Carleer, M. R., Chackerian Jr., C., Chance, K., Coudert, L. H., Dana, V., Devi, V. M., Flaud, J.-M., Gamache, R. R., Goldman, A., Hartmann, J.-M., Jucks, K. W., Maki, A. G., Mandin, J.-Y., Massie, S. T., Orphal, J., Perrin, A., Rinsland, C. P., Smith, M. A. H., Tennyson, J., Tolchenov, R. N., Toth, R. A., Vander Auwera, J., Varanasi, P., and Wagner, G.: The HITRAN 2004 molecular spectroscopic database, J. Quant. Spectrosc. Ra., 96, 139–204, 2005.

Tejwani, G. D. T. and Yeung, E. S.: Pressure broadened linewidths of HNO_3, J. Chem. Phys., 68, 2012–2013, 1978.

Toth, R. A., Brown, L. R., and Cohen, E. A.: Line strengths of nitric acid from 850 to 920 cm^{-1}, J. Molec. Spectrosc., 218, 151–168, 2003.

Zu, L., Hamilton, P. A., and Davies, P. B.: Pressure broadening and frequency measurements of nitric acid lines in the 683 GHz region, J. Quant. Spectrosc. Ra., 73, 545–556, 2002.